AGU PUBLICATIONS

Geophysical Research Letters

RESEARCH LETTER
10.1002/2015GL063105

Key Points:
- Eddies can significantly impact the surface turbulent heat fluxes
- Stronger heat flux anomalies are associated with large-amplitude eddies
- Cyclonic eddies contribute to ocean heat gain, while anticyclonic with heat loss

Supporting Information:
- Texts S1–S3 and Figures S1–S3

Correspondence to:
A. B. Villas Bôas,
avillasboas@ucsd.edu

Citation:
Villas Bôas, A. B., O. T. Sato, A. Chaigneau, and G. P. Castelão (2015), The signature of mesoscale eddies on the air-sea turbulent heat fluxes in the South Atlantic Ocean, *Geophys. Res. Lett.*, *42*, 1856–1862, doi:10.1002/2015GL063105.

Received 11 JAN 2015
Accepted 24 FEB 2015
Accepted article online 26 FEB 2015
Published online 23 MAR 2015

The signature of mesoscale eddies on the air-sea turbulent heat fluxes in the South Atlantic Ocean

A. B. Villas Bôas[1,2], O. T. Sato[1], A. Chaigneau[3,4], and G. P. Castelão[1]

[1]Oceanographic Institute of the University of São Paulo, São Paulo, Brazil, [2]Now at Scripps Institution of Oceanography, University of California, San Diego, La Jolla, California, USA, [3]Institut de Recherche Pour le Développement, Toulouse, France, [4]Laboratoire d'Études en Géophysique et Océanographie Spatiale, UMR, CNRS, CNES, IRD, Paul Sabatier University, Toulouse, France

Abstract By collocating 10 years (1999–2009) of remotely sensed surface turbulent heat fluxes with satellite altimetry data, we investigate the impact of oceanic mesoscale eddies on the latent and sensible heat fluxes in the South Atlantic Ocean. In strongly energetic regions, such as the Brazil–Malvinas confluence and the Agulhas Current Retroflection, eddies explain up to 20% of the total variance in the surface turbulent heat fluxes with averaged anomalies of ± (10–20) W/m^2. Cyclonic (anticyclonic, respectively) eddies are associated with negative (positive) heat flux anomalies that tend to cool (warm) the marine atmospheric boundary layer. A composite analysis of the turbulent heat flux anomalies inside the eddies reveals a direct relationship between eddy amplitude and the intensity of such anomalies. In addition, these anomalies are stronger near the eddy center, decaying radially to reach minimum values outside the eddies.

1. Introduction

The ocean-atmosphere system is primarily turbulent. In the mesoscale band, oceanic eddies play a crucial role in transporting heat, salt, momentum, and biogeochemical tracers along their trajectories, significantly impacting the ocean dynamics and fluxes [*Olson*, 1991; *Wunsch*, 1999; *Morrow et al.*, 2003]. Mesoscale eddies are coherent rotating features with typical horizontal scales of 50–300 km and time scales ranging from weeks to months [*Chelton et al.*, 2011a]. They also exhibit particular thermohaline vertical structures associated with strong dynamical perturbations of the density and pressure fields [*Olson*, 1991; *Chaigneau et al.*, 2011; *Kurian et al.*, 2011; *Zhang et al.*, 2013; *Roullet et al.*, 2014]. These perturbations extend up to the sea surface, leading to anomalies on sea surface height, sea surface temperature (SST), and wind stress, among others [*Frenger et al.*, 2013; *Souza et al.*, 2014]. As a result, it is expected that eddies impact the air-sea fluxes and the overlaying atmospheric circulation [*Frenger et al.*, 2013].

The turbulent latent (LHF) and sensible (SHF) heat fluxes are the primary processes by which the ocean releases heat to the atmosphere [*Cayan*, 1992]. Both the LHF and SHF can be derived from bulk formulae linking oceanic and atmospheric parameters—such as air-specific humidity, SST, and wind speed—to the heat exchanged at the air-sea interface [*Liu et al.*, 1979; *Fairall et al.*, 2003; *Large and Yeager*, 2009]. The anomalies caused by mesoscale eddies in some of these parameters have been recently investigated [e.g., *White and Annis*, 2003; *Hausmann and Czaja*, 2012; *Frenger et al.*, 2013; *Souza et al.*, 2014; *Chelton and Xie*, 2010]. Although there is ample evidence that oceanic mesoscale features have a significant impact on air-sea properties, there is still a lack of knowledge about their signature on the surface turbulent heat fluxes and their potential contributions to the net surface heat budget.

The recent release of daily satellite-based data from the *French Research Institute for Exploitation of the Sea* (IFREMER) [*Bentamy et al.*, 2013] has sufficient resolution to estimate the LHF and SHF associated with mesoscale processes. The present work merges satellite altimetry sea level anomaly (SLA) data with remotely sensed surface heat fluxes to investigate the impact of mesoscale ocean eddies on the LHF and SHF in the South Atlantic Ocean (SA).

The SA encompasses both quiescent areas and two regions of intense energetic variability associated with the presence of large mesoscale eddies (Figure 1a), namely, the Agulhas Current Retroflection (AGR) [*Olson and Evans*, 1986; *Goni et al.*, 1997] and the Brazil-Malvinas confluence (BMC) [*Garzoli and Garraffo*, 1989; *Olson et al.*, 1988]. More specifically, we aim (i) to assess the mean LHF and SHF anomalies induced by cyclonic and anticyclonic eddies in the SA, (ii) to describe the spatial variations of the heat flux anomalies in

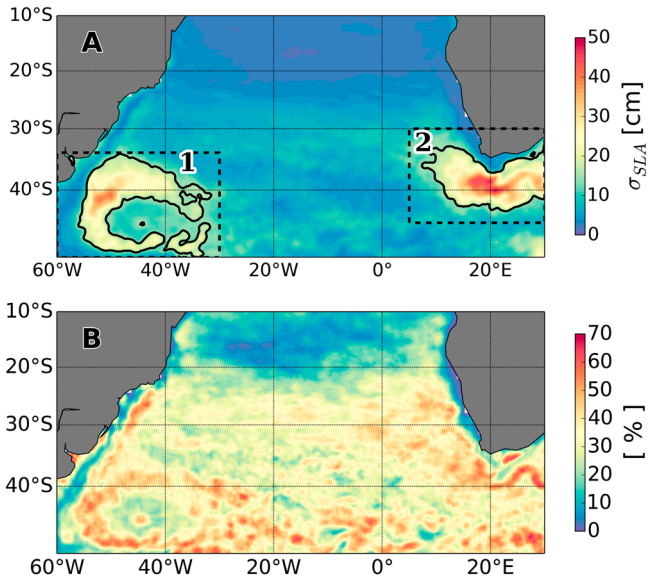

Figure 1. (a) Standard deviation (σ_{SLA}) of the sea level anomaly (SLA). Black solid contours correspond to σ_{SLA} = 15 cm. The dashed boxes delimit the Brazil–Malvinas confluence region (BMC, box 1) and the Agulhas Current Retroflection region (AGR, box 2). (b) Eddy frequency that represents the percentage of time that each grid point was inside an eddy during the whole time series.

the SA and investigate their relationship with eddy amplitudes, and (iii) to depict the distribution of the LHF and SHF anomalies within the eddies.

2. Data and Methods

2.1. Satellite Sea Level Anomaly Data, Eddy Detection, and Tracking

Ten years of altimetric SLA data (1999–2009) from the gridded multimission product by Ssalto/Duacs, distributed by Archiving, Validation, and Interpretation of Satellite Oceanographic data (AVISO) (http://www.aviso.oceanobs.com/duacs/), were used to identify mesoscale eddies in this work. The SLA from AVISO is defined relatively to a 7 year mean (1993–1999), with a nominal precision of 2 cm [*Le Traon et al.*, 2003; *Ducet et al.*, 2000], and it is distributed in a uniform 1/4° grid at 7 day intervals, allowing to monitor mesoscale dynamics in the ocean. On each weekly SLA map, eddies were automatically identified and tracked using the method developed by *Chaigneau et al.* [2008, 2009] that is a threshold free method, based on closed contours of SLA (see supporting information).

2.2. Surface Turbulent Heat Flux Data and Anomalies

Although numerous efforts have been made to improve the assessment of turbulent heat fluxes at the air-sea interface, it is still a challenge to estimate them with great accuracy. Existing heat flux products tend to strongly differ from each other, mostly because of inconsistencies between their input variables and/or methodologies [e.g., *Dong et al.*, 2007; *Santorelli et al.*, 2011; *Pinker et al.*, 2014]. As pointed out by *Santorelli et al.* [2011], in comparison to model–based products, satellite–based products have the advantage of providing nearly global data at relatively high spatiotemporal resolution. In addition, in regions where in situ observations are relatively sparse, such as in the SA [*Garzoli et al.*, 2013; *Garzoli and Matano*, 2011], the accuracy of model-based products is limited by the lack of input data to assimilate.

The latest release (V3) of surface turbulent heat fluxes distributed by IFREMER [*Bentamy et al.*, 2013] combines the bulk algorithms of *Fairall et al.* [2003] with input parameters mainly obtained from remote measurements to estimate the LHF and SHF using bulk formulae. After validation against *in situ* data from buoys, daily LHF and SHF (positive upward) are provided from October 1999 to November 2009, with spatial grid resolution of 0.25° × 0.25°.

The lowest resolution among the input variables used on the *Bentamy et al.* [2013] product is associated with the air temperature (T_{a10}), which is obtained from the European Centre for Medium Range Weather Forecasts reanalyses (ERA-Interim) with 0.75° × 0.75° resolution, and then optimally interpolated onto a 0.25° × 0.25° regular grid. As discussed in section 3, most of the eddies analyzed in the present study have spatial scales of ~140 km (supporting information Figures S1 and S2). Therefore, the LHF and SHF delivered by IFREMER seem promising to estimate the turbulent heat flux anomalies associated with mesoscale eddies. Also, *Desbiolles et al.* [2014] have successfully used the IFREMER product to describe LHF and SHF anomalies during short-term coastal upwelling events on scales of tens of kilometers.

Air-sea fluxes vary over a broad range of spatiotemporal scales [*Gulev and Belyaev*, 2012]. In order to isolate mesoscale features in the turbulent heat fluxes signal, the LHF and SHF data were filtered both in time and space. First, a temporal band-pass Hann window was applied to preserve only periods between 7 and 90 days, which correspond to the typical time scales of the eddies. Second, the data from grid points located

inside the identified eddies were removed from the time-filtered maps. The resultant LHF and SHF maps, characterized by masked data within eddy contours, are then spatially low-pass filtered using a moving average Hann window of 600 km. Thus, these spatially-filtered maps, only contains signals with wavelengths longer than 600 km and are taken as the large-scale reference level. Third, LHF and SHF anomaly maps, associated only with mesoscale features, were obtained by subtracting the large-scale reference level from the time-filtered maps.

This approach allows one to highlight the signature of mesoscale eddies on the surface turbulent heat fluxes even if they are superimposed on large-scale features. The window lengths were chosen in order to smooth as much as possible the large-scale variability without significantly attenuating the variability of the eddies. Note that similar methodologies and window lengths were recently applied to distinct data sets by *Chelton et al.* [2011b], *Gaube et al.* [2014], and *Souza et al.* [2014]. The results discussed hereinafter are based on the LHF and SHF anomaly maps.

Finally, the spatial pattern of the heat flux anomalies inside eddies and their immediate surroundings was estimated using composite maps. For each identified eddy, the LHF and SHF anomalies were interpolated onto a uniform high-resolution grid, normalized by the radial distance from the eddy center to the eddy edge. The spatial extent of the grid was chosen to represent the anomaly fields to a distance twice the eddy radius in each direction. This scaling allows one to average the anomaly of thousands of eddies as a single composite map, consisting of an efficient way to depict their mean signature on surface tracers [*Frenger et al.*, 2013; *Chelton et al.*, 2011b; *Hausmann and Czaja*, 2012].

3. Results and Discussion

For the 10 year studied period (1999–2009), cyclonic and anticyclonic eddies were frequently observed south of ~30°S, particularly near the BMC and AGR regions, where the eddy frequency reaches from 50% to 70% (Figure 1b). In contrast, eddy frequency strongly weakens in the tropical SA between 10°S and 20°S. Typical values of the observed eddy radius and amplitude were between 30 km and 175 km, and 2 cm and 50 cm, respectively, with most eddies having a radius of ~70 km and an amplitude of ~5 cm (supporting information Figures S1–S3). The mean amplitude map exhibits patterns similar to the SLA variability map shown in Figure 1a, indicating that regions with high SLA variability are associated with the presence of large-amplitude eddies.

3.1. Geographical Distribution of the Eddy-Induced Turbulent Heat Fluxes Anomalies in the South Atlantic

In comparison to the rest of the SA basin, the time-averaged heat flux anomalies induced by cyclonic and anticyclonic eddies are remarkably strong in the BMC and AGR regions (Figure 2). Mesoscale eddies are known to have a well-defined imprint on the SST, such that cold-core cyclonic eddies are characterized by negative SST anomalies, while warm-core anticyclonic eddies by positive [e.g., *Frenger et al.*, 2013; *Hausmann and Czaja*, 2012; *Gaube et al.*, 2014]. Yet an anomaly on the SST changes (1) the SHF, by modifying the temperature gradient between the ocean and atmosphere, and (2) the LHF, since the saturation humidity at the sea surface is defined as the amount of moisture that the overlaying air could "hold" for a given SST. Therefore, as suggested by Figure 2, it is expected that anticyclonic eddies contribute on average to positive heat flux anomalies (ocean heat loss), while cyclonic eddies contribute to negative anomalies (ocean heat gain).

On average over the SA, the mean eddy-induced LHF and SHF anomalies are weak and not statistically significant. However, in the BMC and AGR regions these anomalies can reach the same order of magnitude (~10–20 W/m^2), as the amplitude of the large-scale annual cycle, and the variability of the eddies explains up to 20% of the variance in the surface turbulent heat flux signals (Table 1). Thus, although air-sea interactions have been believed to be dominated by large-scale processes [*Bourassa et al.*, 2010; *Frenger et al.*, 2013], these results strongly suggest that eddies can play a significant role on the variability of the surface turbulent heat fluxes, giving evidence of a coupling between ocean and atmosphere at mesoscales, which reinforces the recent findings of *Song et al.* [2009], *Chelton and Xie* [2010], and *Frenger et al.* [2013].

One could question why are the eddy imprints stronger in the eddy-rich regions than in the rest of the basin? *Hausmann and Czaja* [2012] also showed that in the North Atlantic and Southern Ocean, SST anomalies associated with mesoscale eddies are stronger in energetic regions, characterized by high SLA

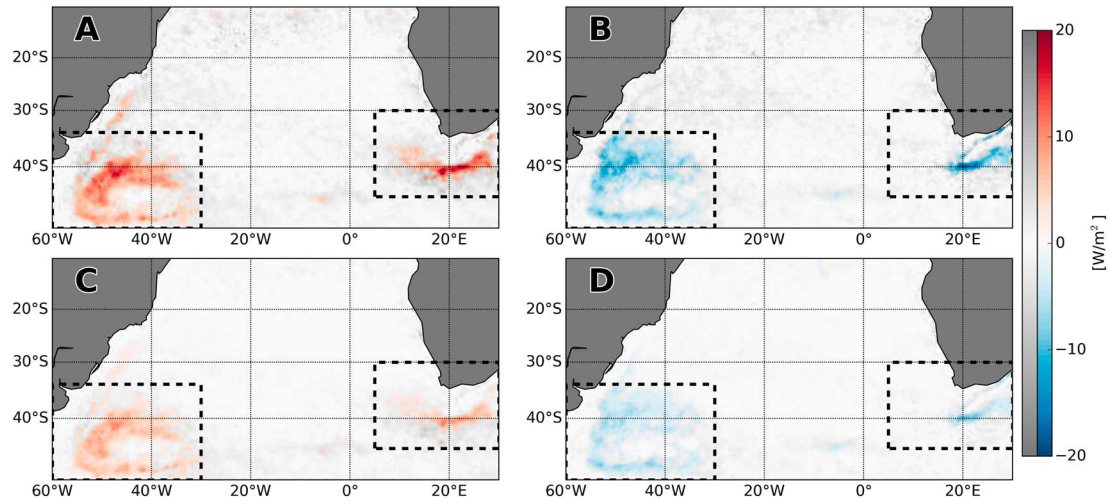

Figure 2. Temporal mean of surface turbulent heat flux anomalies associated with mesoscale eddies in the South Atlantic (positive upward). Mean latent heat flux (LHF) anomalies inside (a) anticyclonic and (b) cyclonic eddies. Mean sensible heat flux (SHF) anomalies inside (c) anticyclonic and (d) cyclonic eddies. Grid points where the mean is not statistically different from zero by at least at one standard error (see supporting information), are shown in gray scale. The dashed lines delimit the BMC and AGR regions.

variability. Since high SLA variability is indeed associated with large-amplitude eddies [*Chelton et al.*, 2011a], we explore instead the dependency of LHF and SHF anomalies on the eddy amplitude.

3.2. Averaged Composite Maps

Composite maps of the LHF and SHF anomalies for cyclonic and anticyclonic eddies were constructed as explained in section 2.2 considering all eddies detected in the SA. Figure 3 shows the maximum absolute value of the anomalies in the averaged composite maps as a function of the respective eddy amplitude. Regardless of the eddy polarity (cyclonic or anticyclonic), the magnitude of the LHF and SHF anomalies increases with the eddy amplitude. The order of magnitude is similar for both eddy types but are negative (positive, respectively) for cyclonic (anticyclonic) eddies. Similarly to what is observed in large-scale averages of surface turbulent heat fluxes over the SA [*Yu and Weller*, 2007], the eddy-induced anomalies on the LHF are larger than on the SHF (Figures 2 and 3).

Considering that the majority of the identified eddies are surface-intensified, cyclones (anticyclones) promote the doming (depression) of the isopycnals, leading to negative (positive) SLA and SST anomalies. The larger the eddy amplitude, the stronger would be the isopycnal deformation, the mixed-layer temperature anomalies [e.g., *Holte et al.*, 2013], and consequently, the turbulent heat flux anomalies. Note that

Table 1. Anticyclonic (Cyclonic): Maximum (Minimum) Values Plus or Minus One Standard Error (See Supporting Information) of the Time-Mean LHF and SHF Anomalies Associated With Anticyclonic (Cyclonic) Eddies Observed in the BMC and AGR Regions[a]

	LHF		SHF	
	BMC	AGR	BMC	AGR
Anticyclonic (W/m^2)	19.2 ±5	20.8 ±8	11.6 ±3.8	11.5 ±5
Cyclonic (W/m^2)	−14.2 ±6	−19.4 ±7	−8.9 ±2.5	−10.5 ± 3.4
Annual Range (W/m^2)	55–93	112–138	7–37	30–50
Exp. Var. (%)	17.5	20	16.2	15

[a]Annual Range: Large-scale LHF and SHF annual cycle, estimated as the minimum and maximum values observed in the monthly average of the original (unfiltered) heat flux data. Exp. Var.: Maximum percentage of the variance of the original (unfiltered) LHF and SHF signals explained by the variance of the anomalies caused by the eddies. All values are statistically significant at the 95% confidence level.

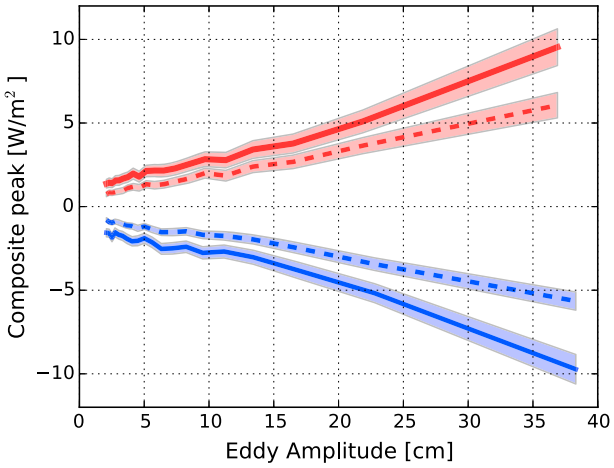

Figure 3. Maximum (minimum, for cyclonic eddies) surface turbulent heat flux anomalies within anticyclonic (red lines) and cyclonic (blue lines) eddies as a function of the respective eddy amplitude. The solid and dashed lines are the LHF and SHF, respectively. The confidence interval at one standard error of the mean is shown in blue and red shadows. The anomalies shown were computed from averaged composite maps as explained in Figure 4.

subsurface-intensified eddies could lead to opposite SST anomalies [e.g., *Chaigneau et al.*, 2011; *Colas et al.*, 2012] and would probably impact turbulent heat fluxes in a different way. However, determining the exact nature of the eddies is beyond the scope of this work and exploring potential differences between anomalies caused by surface and subsurface intensified eddies will deserve future study.

The mean spatial distribution of the surface turbulent heat flux anomalies inside large-amplitude eddies is shown in Figure 4. These composite maps were obtained by averaging heat flux anomalies for eddies with the 5% largest amplitudes (≥27 cm), corresponding to ~4100 cyclonic and ~4000 anticyclonic eddy realizations. Near the center of large-amplitude eddies, the mean LHF and SHF anomalies are of the order of ±10 ±1 W/m^2 and ±6 ±0.6 W/m^2, respectively. The LHF and SHF anomalies decrease outward, reaching minimum values near the eddy edge. From Figure 4, we also note that the maximum anomalies do not coincide with the eddy center but are slightly shifted equatorward (poleward, respectively) for cyclonic (anticyclonic) eddies. This meridional displacement is persistent in composite maps for any other eddy amplitude range (not shown). Similar meridional asymmetries were also observed by

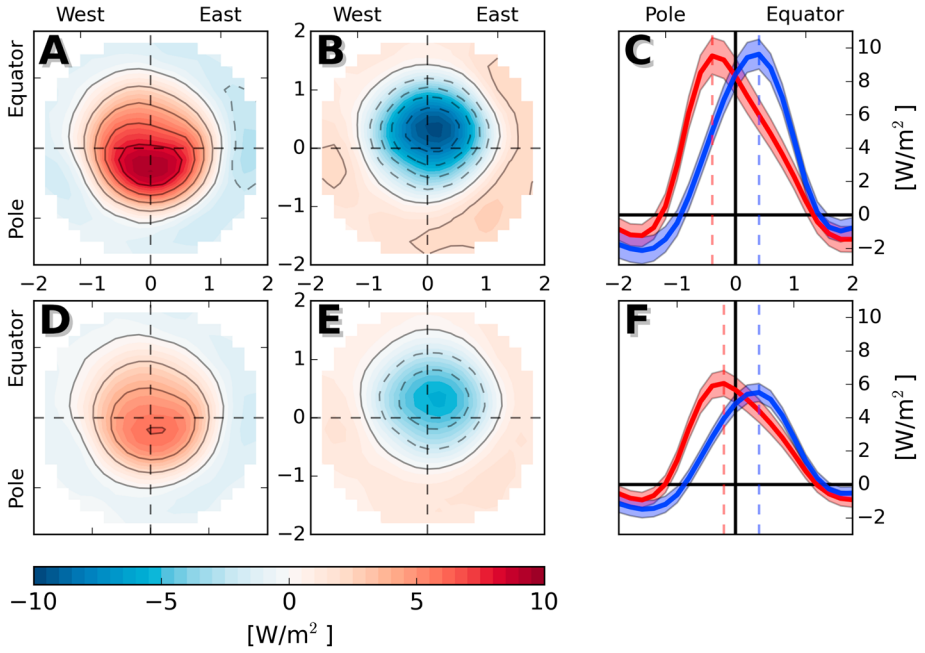

Figure 4. Averaged composite maps of (a, b) LHF and (d, e) SHF anomalies inside anticyclonic (Figures 4a and 4d) and cyclonic (Figures 4b and 4e) eddies. Composite maps were obtained from eddies having the 5% highest absolute amplitudes (≥ 27.3 cm), which corresponds to 4189 cyclonic and 4013 anticyclonic eddy realizations, and 1115 cyclonic and 979 anticyclonic individual eddies (see supporting information). The axes in the composite maps are the normalized distance between the eddy center and twice the eddy edge. Contour intervals are shown every 2 W/m^2. (c, f) The meridional section of the absolute value of the LHF and SHF anomalies, respectively, crossing the composite peak for anticyclonic (red lines) and cyclonic (blue lines) eddies, with the confidence interval at one standard error of the mean shown in blue and red shadows.

Hausmann and Czaja [2012] in composite maps for the SST anomaly in energetic areas. Also, composites of heat content anomaly induced by eddies in the Southern Ocean [*Stephenson et al.*, 2013] appear to have meridional asymmetries consistent to those observed in Figure 4.

As suggested by earlier studies on mesoscale eddy dynamics and propagation [e.g., *Adem*, 1956; *Firing and Beardsley*, 1976; *McWilliams and Flierl*, 1979], as the ambient fluid parcels rotate with the eddy, they undergo a change in planetary vorticity due to the β effect. In order to preserve their potential vorticity, fluid parcels at the northern and southern flanks of the eddy will then compensate the planetary vorticity change by modifying their relative vorticity. In the Southern Hemisphere, this results in a weak vorticity anomaly dipole that induce upwelling in the northern flank of cyclonic eddies and downwelling in the southern flank. Thus, in cold-core cyclonic eddies, the cooler water brought up by the upwelling would enhance the negative heat flux anomalies in the northern flank, as observed in Figure 4. The opposite would happen to anticyclonic eddies, producing enhanced positive heat fluxes in the southern flank of the eddies.

4. Summary and Concluding Remarks

From 10 years of satellite altimetry and remote-sensed heat flux estimations, we have provided further evidence for the coupling between ocean and atmosphere at mesoscales. Turbulent heat flux anomalies associated with cyclonic (anticyclonic) eddies are negative (positive), indicating ocean heat gain (loss). On average over the SA, the time mean LHF and SHF anomalies induced by mesoscale eddies are weak, but they strongly increase in energetic regions such as the BMC and AGR, reaching up to 10–20 W/m^2. In those regions such anomalies can have the same order of magnitude as the amplitude of the seasonal cycle, and eddies explain up to 20% of the total variance of the surface turbulent heat fluxes.

As shown by *Stephenson et al.* [2013], anomalies in the air-sea heat fluxes are an important source of variability in the Southern Ocean upper ocean heat content. Also, *Dong et al.* [2007] have found an imbalance on the mixed-layer heat budget near the BMC and AGR regions. Our results suggest that the contribution of eddies to the surface heat fluxes is nonnegligible. Therefore, it should be taken into account to allow for a better understanding and representation of the processes governing the upper ocean heat budgets.

Composite maps of thousands of eddies in the SA revealed a well-defined quasi-circular imprint within the eddy interior, with relatively strong turbulent heat flux anomalies ($\pm$10 W/m^2) near the center of the most energetic eddies, decaying radially outward. However, maximum LHF and SHF anomalies are slightly shifted equatorward (poleward) for cyclonic (anticyclonic) eddies, which could be explained by the β effect. The intensity of these anomalies increases with the eddy amplitude, indicating that large-amplitude eddies have a stronger impact on the surface turbulent heat fluxes than small-amplitude eddies.

Energy exchanges between mesoscale eddies and the overlaying atmosphere could impact the eddy decay rate and lifetime. Moreover, the signature of a recently formed eddy on the SST could be progressively eroded by surface heat fluxes, that act to minimize the air-sea gradients. Thus, stronger LHF and SHF anomalies are preferentially observed in regions of eddy genesis, such as the BMC and AGR. Further investigations on the evolution of such anomalies following individual eddies are needed in order to better understand how the air-sea heat fluxes change during the eddy life cycles and how they affect the eddy decay rate. Owing to the intensity of the heat flux anomalies, eddies could impact beyond the atmospheric boundary layer, having potential implications on the large-scale atmospheric circulation, as previously suggested by *Chelton and Xie* [2010]. Hence, coupled climate models should be capable to represent air-sea interactions at mesoscales to enhance the accuracy of their predictions.

Acknowledgments
We acknowledge the anonymous reviewers for their helpful comments. This research was funded by the São Paulo Research Foundation (FAPESP) on grants 2012/21243–6, 2013/02355–0, 2013/11825–0, and 2008/58101–9. The authors would like to thank to the *Archiving, Validation and Interpretation of Satellite Oceanographic data* (AVISO) for providing the altimetric product used in this work and the *Institut Français de Recherche pour l'Exploitation de la Mer* (IFREMER) for the turbulent heat fluxes data. This work is also a contribution to the joint CNES/NASA OSTST project "Merging of satellite and in situ observations for the analysis of meso and submesoscale dynamics."

The Editor thanks two anonymous reviewers for their assistance in evaluating this paper.

References

Adem, J. (1956), A series solution for the barotropic vorticity equation and its application in the study of atmospheric vortices, *Tellus*, *8*(3), 364–372.

Bentamy, A., S. A. Grodsky, K. Katsaros, A. M. Mestas-Nuñez, B. Blanke, and F. Desbiolles (2013), Improvement in air-sea flux estimates derived from satellite observations, *Int. J. Remote Sens.*, *34*(14), 5243–5261.

Bourassa, M. A., S. T. Gille, D. L. Jackson, J. B. Roberts, and G. A. Wick (2010), Ocean winds and turbulent air-sea fluxes inferred from remote sensing, *Oceanography*, *23*(4), 36–51.

Cayan, D. R. (1992), Latent and sensible heat flux anomalies over the northern oceans: Driving the sea surface temperature, *J. Phys. Oceanogr.*, *22*(8), 859–881.

Chaigneau, A., A. Gizolme, and C. Grados (2008), Mesoscale eddies off Peru in altimeter records: Identification algorithms and eddy spatio-temporal patterns, *Prog. Oceanogr.*, *79*(2–4), 106–119, doi:10.1016/j.pocean.2008.10.013.

Chaigneau, A., G. Eldin, and B. Dewitte (2009), Eddy activity in the four major upwelling systems from satellite altimetry (1992–2007), *Prog. Oceanogr.*, *83*(1–4), 117–123, doi:10.1016/j.pocean.2009.07.012.
Chaigneau, A., M. Le Texier, G. Eldin, C. Grados, and O. Pizarro (2011), Vertical structure of mesoscale eddies in the eastern South Pacific Ocean: A composite analysis from altimetry and Argo profiling floats, *J. Geophys. Res.*, *116*, C11025, doi:10.1029/2011JC007134.
Chelton, D. B., and S.-P. Xie (2010), Coupled ocean-atmosphere interaction at oceanic mesoscales, *Oceanography*, *23*(4), 52–69.
Chelton, D. B., M. G. Schlax, and R. M. Samelson (2011a), Global observations of nonlinear mesoscale eddies, *Prog. Oceanogr.*, *91*, 167–216.
Chelton, D. B., P. Gaube, M. G. Schlax, J. J. Early, and R. M. Samelson (2011b), The influence of nonlinear mesoscale eddies on near-surface oceanic chlorophyll, *Science*, *334*(6054), 328–332.
Colas, F., J. C. McWilliams, X. Capet, and J. Kurian (2012), Heat balance and eddies in the Peru-Chile current system, *Clim. Dyn.*, *39*(1–2), 509–529.
Desbiolles, F., B. Blanke, and A. Bentamy (2014), Short-term upwelling events at the western African coast related to synoptic atmospheric structures as derived from satellite observations, *J. Geophys. Res. Oceans*, *119*, 461–483, doi:10.1002/2013JC009278.
Dong, S., S. T. Gille, and J. Sprintall (2007), An assessment of the Southern Ocean mixed layer heat budget, *J. Clim.*, *20*(17), 4425–4442.
Ducet, N., P.-Y. Le Traon, and G. Reverdin (2000), Global high-resolution mapping of ocean circulation from TOPEX/Poseidon and ERS-1 and -2, *J. Geophys. Res.*, *105*(C8), 19,477–19,498, doi:10.1029/2000JC900063.
Fairall, C., E. F. Bradley, J. Hare, A. Grachev, and J. Edson (2003), Bulk parameterization of air-sea fluxes: Updates and verification for the COARE algorithm, *J. Clim.*, *16*(4), 571–591.
Firing, E., and R. C. Beardsley (1976), The behavior of a barotropic eddy on a β-plane, *J. Phys. Oceanogr.*, *6*(1), 57–65.
Frenger, I., N. Gruber, R. Knutti, and M. Münnich (2013), Imprint of Southern Ocean eddies on winds, clouds and rainfall, *Nat. Geosci.*, *6*(8), 608–612.
Garzoli, S. L., and Z. Garraffo (1989), Transports, frontal motions and eddies at the Brazil-Malvinas currents confluence, *Deep Sea Res., Part A*, *36*(5), 681–703.
Garzoli, S. L., and R. Matano (2011), The South Atlantic and the Atlantic meridional overturning circulation, *Deep Sea Res., Part II*, *58*(17), 1837–1847.
Garzoli, S. L., M. O. Baringer, S. Dong, R. C. Perez, and Q. Yao (2013), South Atlantic meridional fluxes, *Deep Sea Res., Part I*, *71*, 21–32.
Gaube, P., D. B. Chelton, R. M. Samelson, M. G. Schlax, and L. W. O'Neill (2014), Satellite observations of mesoscale eddy-induced Ekman pumping, *J. Phys. Oceanogr.*, *45*, 104–132.
Goni, G. J., S. L. Garzoli, A. J. Roubicek, D. B. Olson, and O. B. Brown (1997), Agulhas ring dynamics from TOPEX/POSEIDON satellite altimeter data, *J. Mar. Res.*, *55*(5), 861–883.
Gulev, S. K., and K. Belyaev (2012), Probability distribution characteristics for surface air-sea turbulent heat fluxes over the global ocean, *J. Clim.*, *25*(1), 184–206.
Hausmann, U., and A. Czaja (2012), The observed signature of mesoscale eddies in sea surface temperature and the associated heat transport, *Deep Sea Res., Part I*, *70*, 60–72.
Holte, J., F. Straneo, C. Moffat, R. Weller, and J. T. Farrar (2013), Structure and surface properties of eddies in the Southeast Pacific Ocean, *J. Geophys. Res. Oceans*, *118*, 2295–2309, doi:10.1002/jgrc.20175.
Kurian, J., F. Colas, X. Capet, J. C. McWilliams, and D. B. Chelton (2011), Eddy properties in the California current system, *J. Geophys. Res.*, *116*, C08027, doi:10.1029/2010JC006895.
Large, W., and S. Yeager (2009), The global climatology of an interannually varying air-sea flux data set, *Clim. Dyn.*, *33*(2–3), 341–364.
Le Traon, P., Y. Faugère, F. Hernandez, J. Dorandeu, F. Mertz, and M. Ablain (2003), Can we merge GEOSAT follow-on with TOPEX/Poseidon and ERS-2 for an improved description of the ocean circulation?, *J. Atmos. Oceanic Technol.*, *20*(6), 889–895, doi:10.1175/1520-0426(2003)020<0889:CWMGFW>2.0.CO;2.
Liu, W. T., K. B. Katsaros, and J. A. Businger (1979), Bulk parameterization of air-sea exchanges of heat and water vapor including the molecular constraints at the interface, *J. Atmos. Sci.*, *36*(9), 1722–1735.
McWilliams, J. C., and G. R. Flierl (1979), On the evolution of isolated, nonlinear vortices, *J. Phys. Oceanogr.*, *9*(6), 1155–1182.
Morrow, R., F. Fang, M. Fieux, and R. Molcard (2003), Anatomy of three warm-core Leeuwin Current eddies, *Deep Sea Res., Part II*, *50*(12), 2229–2243.
Olson, D. B. (1991), Rings in the ocean, *Annu. Rev. Earth Planet. Sci.*, *19*, 283–311.
Olson, D. B., and R. H. Evans (1986), Rings of the Agulhas Current, *Deep Sea Res., Part A*, *33*(1), 27–42.
Olson, D. B., G. P. Podestá, R. H. Evans, and O. B. Brown (1988), Temporal variations in the separation of Brazil and Malvinas currents, *Deep Sea Res., Part A*, *35*(12), 1971–1990.
Pinker, R. T., A. Bentamy, K. Katsaros, Y. Ma, and C. Li (2014), Estimates of net heat fluxes over the Atlantic Ocean, *J. Geophys. Res. Oceans*, *119*, 410–427, doi:10.1002/2013JC009386.
Roullet, G., X. Capet, and G. Maze (2014), Global interior eddy available potential energy diagnosed from Argo floats, *Geophys. Res. Lett.*, *41*, 1651–1656, doi:10.1002/2013GL059004.
Santorelli, A., R. Pinker, A. Bentamy, K. Katsaros, W. Drennan, A. Mestas-Nuñez, and J. Carton (2011), Differences between two estimates of air-sea turbulent heat fluxes over the Atlantic Ocean, *J. Geophys. Res.*, *116*, C09028, doi:10.1029/2010JC006927.
Song, Q., D. B. Chelton, S. K. Esbensen, N. Thum, and L. W. O'Neill (2009), Coupling between sea surface temperature and low-level winds in mesoscale numerical models, *J. Clim.*, *22*(1), 146–164.
Souza, J., B. Chapron, and E. Autret (2014), The surface thermal signature and air–sea coupling over the Agulhas rings propagating in the South Atlantic Ocean interior, *Ocean Sci.*, *10*(4), 633–644.
Stephenson, G. R., S. T. Gille, and J. Sprintall (2013), Processes controlling upper-ocean heat content in Drake Passage, *J. Geophys. Res. Oceans*, *118*, 4409–4423, doi:10.1002/jgrc.20315.
White, W. B., and J. L. Annis (2003), Coupling of extratropical mesoscale eddies in the ocean to westerly winds in the atmospheric boundary layer, *J. Phys. Oceanogr.*, *33*, 1095–1107.
Wunsch, C. (1999), Where do ocean eddy heat fluxes matter?, *J. Geophys. Res.*, *104*(C6), 13,235–13,249.
Yu, L., and R. A. Weller (2007), Objectively analyzed air-sea heat fluxes for the global ice-free oceans (1981-2005), *Bull. Am. Meteorol. Soc.*, *88*(4), 527–539.
Zhang, Z., Y. Zhang, W. Wang, and R. X. Huang (2013), Universal structure of mesoscale eddies in the ocean, *Geophys. Res. Lett.*, *40*, 3677–3681, doi:10.1002/grl.50736.